Al-Nahrain Journal of Science
ANJS, Vol. 28(2), June, 2025, pp. 32-47

Theoretical Approach to Evaluate the Effectiveness of Pyridinium Salts in Preventing Mild Steel Corrosion in Acidic Conditions

Shayma M. Ahmad[1,*], Mehdi Salih Shihab[1], Mohammed Moayed Ahmed[1], Alaa Adnan Rashad[1], Omaymah Alaysuy[2]

[1]Department of Chemistry, College of Science, Al-Nahrain University, P. O. Box: 64021, Baghdad, Iraq
[2] Department of Chemistry, College of Science, University of Tabuk, 71474, Tabuk, Saudi Arabia

Article's Information

Received: 16.09.2024
Accepted: 22.04.2025
Published: 15.06.2025

Keywords:
Pyridinium salts
adsorption phenomenon
molecular simulation

Abstract

Pyridinium salts (namely 4-(2-(3-phenylallylidene) hydrazine-1-carbothioamido)-1-propylpyridin-1-ium bromide, A1; 3-(2-(4-(dimethylamino) benzylidene) hydrazine-1-carbothioamido)-1-ethylpyridin-1-ium bromide, A2; 3-(2-(4-(dimethylamino) benzylidene) hydrazine-1-carbothioamido)-1-propylpyridin-1-ium bromide, A3 were successfully prepared in advance, and in this study, they were examined theoretically to determine their effectiveness and efficiency as powerful mild steel corrosion inhibitors. The weight loss method was used to evaluate corrosion inhibition of these salts in 1M H_2SO_4 media which carried out for 24 hours at room temperature. At a variety of pyridinium salt concentrations, the inhibitory efficiency results for all these salts (A1, A2, and A3) were high. The rate of corrosion is known to decrease with increasing inhibitor concentration, while at the same time, surface degree of coverage and inhibition efficiency are rising. The physisorption effects for these prepared compounds (A1, A2, and A3) were indicated by the adsorption results. For the three inhibitors under study, semi-empirical molecular orbital computations and the molecular mechanics approach were used to examine the relationship between experimental and theoretical data. To comprehend the nature of the interaction between the organic inhibitor molecules with the metal surface, theoretical simulations were performed.

http://doi.org/10.22401/ANJS.28.2.04
*Corresponding author: shaymaa.mohsin@nahrainuniv.edu.iq

1. Introduction

Corrosion process is an electrochemical reaction between the metal and its environment which leads to deterioration of metal properties and it causes several effects like the surfaces of national infrastructure, wastewater treatment plants, bridges, and almost on all metallic objects [1]. Iron is one of the popular materials in construction industry with wide range of applications, therefore, the comprehensive analysis and evaluation of various studied corrosion inhibitors were applied to reduce and prevent corrosion reactions on the surface of iron [2-5]. The inhibitors reduce and prevent erosion reaction by adding a little amount of concentration to the environment of erosive [6], this inhibition could be achieved by forming monomolecular film adsorbed surface [7], which blocks the direct contact between metal and corrosive environments [8], [9]. Hetroatoms (N, P, O) which are present in organic chemical compounds have been proven to have an effective effect on the process of corrosion inhibition [10], and thus act as a shield to inhibit this process. Several research works are carried out by using computational design systems of different organic molecules to prevent the corrosion of metals [11], [12]. The aim of this work was to obtain an approach to understanding the nature of interacting the organic compounds when to be next to metal surfaces at acidic environment. Computational methods are of great importance in studying the reduction of the corrosion process because it is an effective method in developing the study of inhibitors and their use in industrial applications. In this paper, quantum chemical

calculations would be performed on three compound salts. These salts as depicted in Figure 1. Molecular parameters calculated were correlated to obtain inhibitory activities for these pyridinium salts.

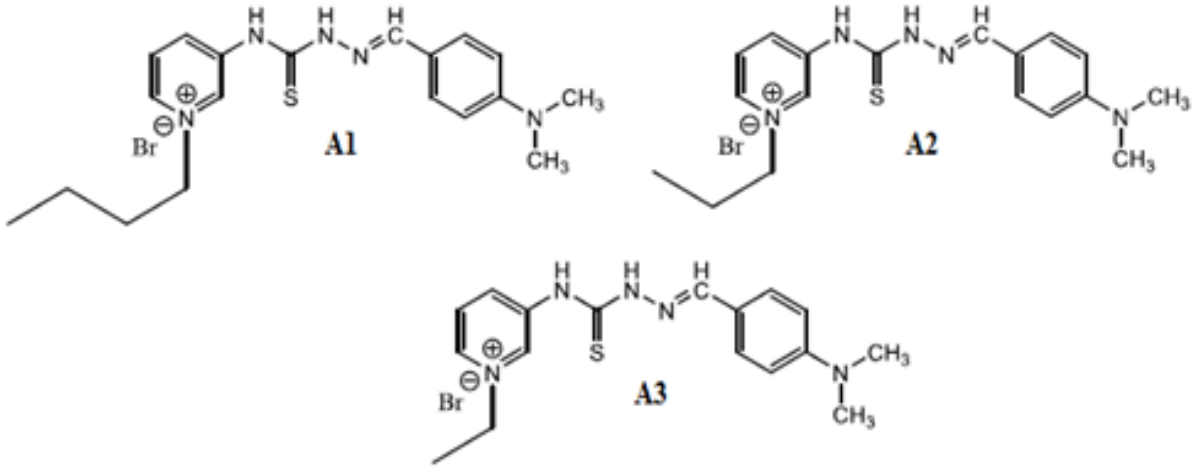

Figure 1: The formula of prepared inhibitor molecules.

2. General synthesis procedure of triethylammonium compounds

Pyridinium salts, namely: 4-(2-(3-phenylallylidene)hydrazine-1-carbothioamido)-1-propylpyridin-1-ium bromide, **A1**; 3-(2-(4-(dimethylamino) benzylidene)hydrazine-1-carbothioamido)-1-ethylpyridin-1-ium bromide, **A2** and 3-(2-(4-(dimethylamino)benzylidene)hydrazine-1-carbothioamido)-1-propylpyridin-1-ium bromide, **A3** were previously synthesized (Scheme 1) [13] :

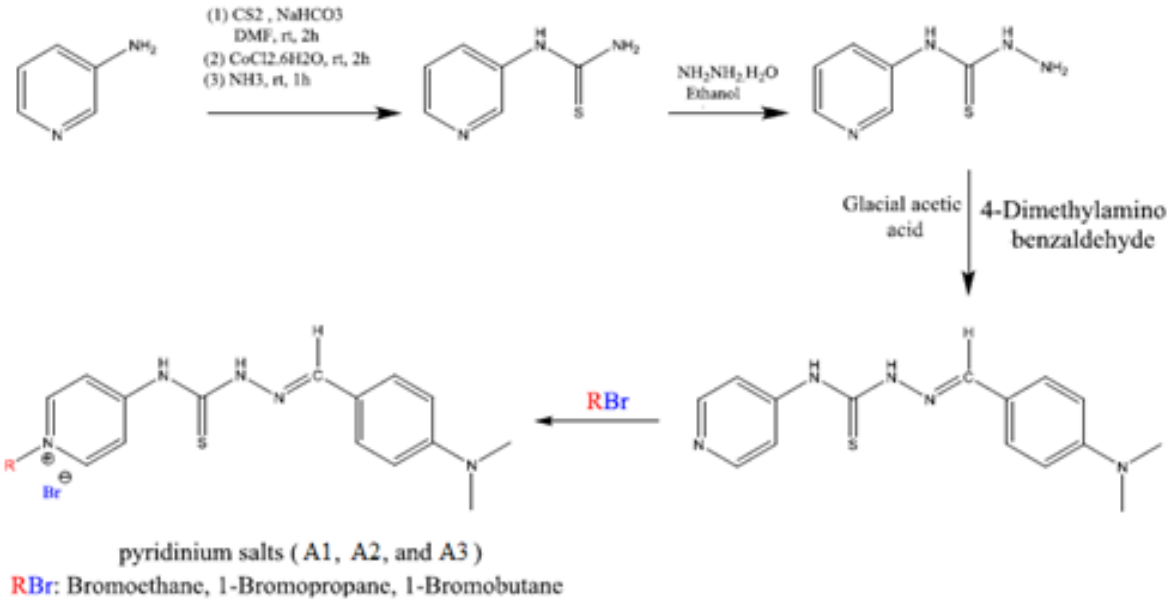

Scheme 1: The pyridinium salts' **A1**–**A3** synthesis

2.1. Preparation of aggressive solution

Solution of (98%) H_2SO_4 (it is diluted with distilled water to get a solution of 1M H_2SO_4). The concentrations that have proven effective as inhibitors were from $5x10^{-4}$ to $1x10^{-2}$ M in the presence 1M of H_2SO_4.

2.2. Weight loss measurements

The mild steel specimen was with composition of following: 0.288 % Mn, 0.0154 % S, 0.03 % C, 0.0199 % Cr, 0.065 % Cu, 0.002% P, and 0.0005 % V, 0.002 % Mo, and remaining Fe. Discs with a diameter of 2.5 cm were obtained from the cutting of mild steel

sheets. Different emery papers were used to obtain smooth surfaces of these discs. After that, the mild steel specimens were cleaned by using distilled water, ethanol, and acetone, respectively. In the beginning, specimens were dried by using a desiccator before corrosion tests. In the first step, an electronic balance was used to weigh the steel disc. In the presence and absence of the known concentration of prepared organic inhibitor, the mild steel disc was immersed in 1M sulfuric acid. After that, it was washed with a sufficient amount of water and acetone after being exposed to room temperature for 24 hours, and then it was re-weighed after drying and kept by using a desiccator. The average weight loss value was tested twice according to the ASTM test [14] for the purpose of ensuring the accuracy of the results using the weight loss method, and thus the average corrosion rate ($mgcm^{-2}h^{-1}$) was calculated. The formula (1) was used to calculate the corrosion rate of mild steel was as a following [15]:

$$W = \frac{\Delta m}{St} \qquad \dots (1)$$

where W = corrosion rate ($mgcm^{-2}h^{-1}$), Δm = difference of weight loss (mg) prior to and after immersion of specimen, S = sample area (cm^2) and t = immersion time (h). Equation 2 is used to calculate the inhibition efficiency (IE%) as following [16]:

$$IE\% = \frac{W_{corr} - W_{corr(inh)}}{W_{corr}} x100 \qquad \dots (2)$$

where W_{corr} and $W_{corr(inh)}$: corrosion rates in both absence and presence of the inhibitor respectively.

2.3. Theoretical Calculations

Correlation has been studied between experimental data and theoretical calculations via inhibition efficiencies for mild steel corrosion process in acidic environment [17, 18]. The study clearly aims to understand the electronic form of some prepared chemical inhibitors using quantitative calculations, while from experimental data the relation between the reactivity of the molecular shape and the efficiency of the inhibition is known. Molecular mechanics was used for the purpose of theoretical calculations at MM+ level, while in the PM3 method used to perform semi-experimental calculations for organic inhibitor molecules in the gas phase and without restrictions at a temperature of 25°C. So, the HyperChem 7.52 Program [20], which has a full geometry improvement, was used for this purpose. To know the inhibition efficiency of synthesized inhibitors, there is a simple method such as the energies of the highest occupied molecular orbital (HOMO) and the lowest unoccupied molecular orbital (LUMO) to analyze calculated parameters. While the PM3 method used to calculate frontier orbital energy gap (ΔE), molecular dipole moment (μ), polarizability (α), electron affinity (A), ionization potential (I), electronegativity (χ), global hardness (η), softness (σ), the fraction of electron transferred (ΔN), electrophilicity index (ω), nucleophilicity index (ε) and back-donation ($\Delta E_{back\text{-}donation}$) (see Table 1). According to Koopman's theorem and Fukui indices [21], these quantum approximated calculated parameters have used to clearly know the properties and reactivity of the synthesized pyridinium salts (A1-A3). As well as, helping to make a correlation between the quantum calculated parameters and experimental data which is obtained by loss weight method for the corrosion process [22].

Table 1: Quantum approximated calculated parameters as following relationships.

$I=-E_{HOMO}$	$A=-E_{LUMO}$	$\Delta E=E_{LUMO}-E_{HOMO}$	$\chi = \frac{I+A}{2}$
$\eta = \frac{I-A}{2}$	$\omega = \frac{\chi^2}{2\eta}$	$\varepsilon = \frac{1}{\omega}$	$\Delta N = \frac{\chi_{Fe} - \eta_{inh}}{2(\eta_{Fe} + \eta_{inh})}$
$\sigma = \frac{1}{\eta}$	$\Delta E_{back-donation} = \frac{E_{LUMO} - E_{HOMO}}{8} = -\frac{\eta}{4}$		

where χFe and χ_{inh} represent the inhibitor molecule's and the metal's respective absolute electronegativity. The absolute hardness of iron is denoted by χFe, whereas the inhibitor molecule is represented by η_{inh}. Since they are softer than the metallic atoms, it is assumed that for a metallic bulk (I = A), χFe = 7.0 eV and ηFe = 0 for the calculation of the electron transmitted (ΔN) [23]. Thus, the electron transport is driven by the difference in electronegativity, and the total

hardness characteristics serve as a resistance [23]. The MM+ force field developed by Hyperchem, which is derived from Allinger's MM2, is explained and compared to other MM2 versions in terms of the conjugation process, the rotation, and structural energy differences. It may also be used to quantify the forces that exist between and within molecules[24]. At atmospheric pressure, iron can be found in two distinct crystal structures: the body centered cubic (bcc), which is stable in the ground state, and the face centered cubic (fcc) [25]. A typical metallic surface was prepared by using iron crystal surface obtained from the crystal shape of iron. The surface was optimized to smallest energy utilizing the Hyperchem's MM+ force field. Unit cells (11×3) of Fe crystal surface were built, and from the optimized crystal surface as an adsorbance surface for inhibitor molecules. The inhibitor compound synthesized to be adsorbate and react with surface particles of the metal crystal surface by adsorption locator module (adsorption locator module identifies possible adsorption sites by carrying Hyperchem's Mm+ force field searches of the configurational space of the substrate-adsorbate). A suitable distance between the adsorbate and the chosen iron crystal surface for optimization by Hyperchem's Mm+ force field was maintained.

3. Results and Discussion

3.1. Synthesis of pyridinium salts A1–A3

Some pyridinium salts, namely: 4-(2-(3-phenylallylidene)hydrazine-1-carbothioamido)-1-propylpyridin-1-ium bromide, A1; 3-(2-(4-(dimethylamino) benzylidene)hydrazine-1-carbothioamido)-1-ethylpyridin-1-ium bromide, A2; 3-(2-(4-(dimethylamino)benzylidene)hydrazine-1-carbothioamido)-1-propylpyridin-1-ium bromide, A3 were previously prepared and thoroughly analyzed by our research group[13].

3.2. In this study of corrosion

After immersing mild steel for 24 hours at room temperature, the deterioration was determined. Measurements of weight loss method was used to obtain the rate of corrosion and effectiveness of inhibition by using different concentrations of inhibitor compounds (A1-A3) which are mentioned in table below (see Table 2) [13]. Table 2 demonstrates that when the concentration of the inhibitor is raised, the corrosion efficiency increases and reaches high inhibition efficiencies at 10^{-2} M. Consequently, of the contrast, the ability of inhibition that follows the order (A2>A1>A3) could be comparable. The effects of carbon chain in the molecular organic structures (that could make flexible structure with A2 and rigidity with A1 and A3) on inhibition efficiency may be explained by values of the inhibition ability [26], as well as, the procedure adsorption of organic molecules on the metal surface. Basic information of method adsorption can elutriate the natural activity which occur on the surface of metal and chemical molecular compound. Therefore, the values of plane coverage degree (θ), with various inhibitor of concentration was achieved by weight loss tests with 1 M sulfuric acid by the surface coverage degree, (θ= IE(%)/100)) (see Table 2) at room temperature, the Equation 3 below shows the relationship between surface coverage degree and concentrations inhibitor to calculate [27]:

$$\frac{C}{\theta} = \frac{1}{K_{ads}} + C \qquad \ldots(3)$$

where C is concentration of inhibitor (M), K_{ads} is the value of equilibrium constant (M^{-1}).

The values of K_{ads} were computed from the crossings of the straight line of C/θ vs concentration, in accordance with the Langmuir isotherm. Equation (4) was used to calculate the values of ΔG^{o}_{ads} [27]: (the molar concentration of water is 55.5 M).

$$K_{ads} = \frac{1}{55.5} exp\left(-\frac{\Delta G^{\circ}_{ads}}{RT}\right) \qquad \ldots(4)$$

Table 3 shows the values of free energy in the adsorption procedure which carries the negative sign to show that the processes of adsorption for the compounds (A1-A3) is spontaneously operation over plane of mild steel in 24 hrs of dipping at room temperature. This approach was used to introduce a clear picture in order to observe the interaction between metal surface and organic molecules (A1-A3). In the environment of corrosion reaction, moving toward the metal surface, organic compounds cause molecules' electrons to interfere with the vacant orbitals on the surface atoms [28, 29], as well as a process known as retro-donation mechanism [30]. The presence of donor atoms in the inhibitor makes the adsorption process more complicated between the inhibitor molecules and the metal, as shown below in equations (5,6) [31,32]:

$$Fe + xH_2O \rightarrow Fe(H_2O_{ads})_x \qquad \ldots(5)$$

$$Fe(H_2O_{ads})_x + Inh_{sol} \rightarrow Fe\text{-}Inh\ complex + xH_2O \qquad \ldots(6)$$

Table 2: Weight loss at room temperature for 24 hour period is measured together with the rate of corrosion, capacity of inhibition (IE%), coverage of surface (θ), and $\Delta G°_{ads}$ for mild steel tested with 1 M sulfuric acid.

Concentration (M)	The rate of corrosion ($mg.cm^{-2}.h^{-1}$)	IE%	θ	ΔG°ads ($kJ.\ mol^{-1}$)
Blank	4.1995			
A1				
5×10^{-4}	1.1367	72.93	0.7293	-31.05 (R^2 = 0,9999)
1×10^{-3}	0.4594	89.06	0.8906	
5×10^{-3}	0.0429	98.97	0.9897	
1×10^{-2}	0.0120	99.71	0.9971	
A2				
5×10^{-4}	0.9132	78.25	0.7825	-31.41 (R^2 = 0,9999)
1×10^{-3}	0.4576	89.10	0.8910	
5×10^{-3}	0.0481	98.85	0.9885	
1×10^{-2}	0.0084	99.79	0.9979	
A3				
5×10^{-4}	1.1754	72.01	0.7201	-30.71 (R^2 = 0,9999)
1×10^{-3}	0.5640	86.56	0.8656	
5×10^{-3}	0.1445	96.55	0.9655	
1×10^{-2}	0.0624	98.51	0.9851	

In addition, it's possible that the quantity of metal complexes present on the metal surface are lower at low concentrations of the prepared organic inhibitor. Therefore, it's obvious that inhibition efficiency is increased with increasing organic inhibitor concentrations. Adsorption inhibitor mechanism works by acting of adsorption compounds via (N and S) atoms that contain organic molecular inhibitor. According to reports, functional groups inside molecules contribute to the electron density distribution of molecules, which can have a significant impact on the process of adsorption on metal surface [33]. To avoid or stop the loss of metal atoms from the surface that can be caused by the reaction of electrochemical dissolutions, through thin film complexes, the organic inhibitors (A1–A3) that the active anode sites were accepting by adsorbing with the metal surface. The values of ΔG^{o}_{ads} for (A1-A3) are listed in Table 2 revealed physical adsorption that occurs physically and electrostatically, via the interaction between the organic molecules and the charged centers on the electrode metal surface and metal surface itself [34]. The organic inhibitor (A2) was showed value ΔG^{o}_{ads} = -31.4 kJ/mol, this was confirmed by IE% readings (78-99) at the various concentrations and indicated in Table 2. At the high concentration of inhibitor, IE% of (A1-A3) are compatible with the values of ΔG^{o}_{ads}, follows the order A2>A1>A3. We believe the reason behind is the molecular structure of a variant carbon chain on the N atom of pyridinium ring and the spatial geometry of (A1-A3) that cause the electron density around the organic molecule to be differed in intensity. Therefore, by comparing the regular distributions of electron densities of molecules with the surface metal to molecules (A3 and A1), the interaction between the molecule (A2) with the surface metal is expected to improve.

3.3. Theoretical Investigation

A correlation between the produced inhibitors experimental inhibitory efficacy and their molecular structure model was determined by semi-empirical calculations involving PM3 level. For the suggested inhibitors of the pyridinium salts (A1), (A2), and (A3), all theoretical calculations were carried out by using more stable of energetically conformations, which are demonstrated to be planar over the entire molecular model of the inhibitors that are recommended and caused by π-systems (see Figure 2).

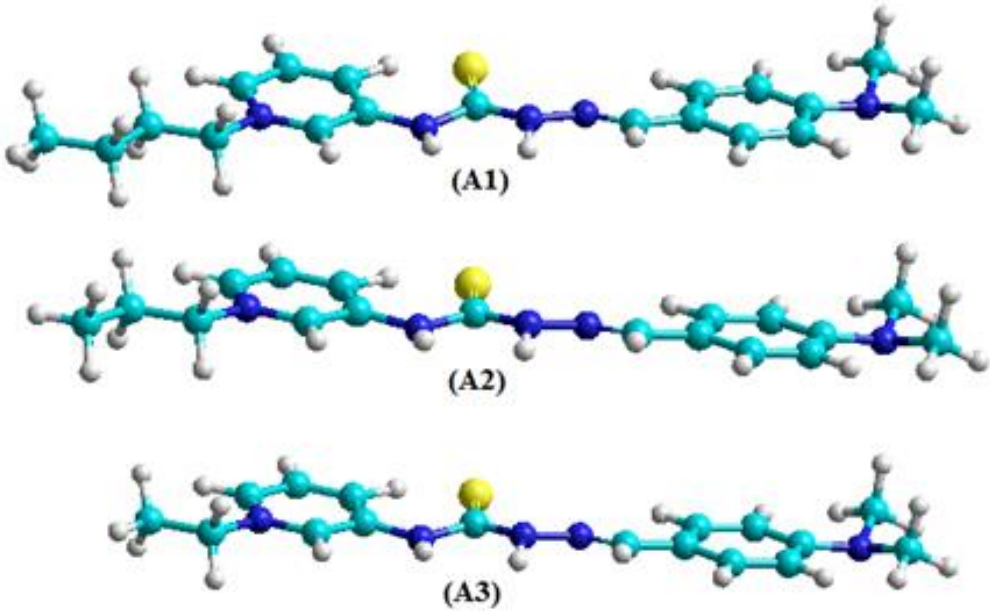

Figure 2: Conformations of the proposed pyridinium salt **A1**–**A3** inhibitors that are energetically stable with PM3 method.

Figure 3 shows the HOMO and LUMO isosurface maps for the proposed inhibitors of (A1), (A2), and (A3). The electronic density of the HOMO and LUMO is entirely concentrated on the N and S atoms present in the proposed inhibitors for all compounds. Accordingly, the electronic density of S and N atoms in the molecular system (except N atom of pyridinium ring) act as a donor for the intermolecular interaction with the environmental metal surface (Fe^0 and Fe^{II}).

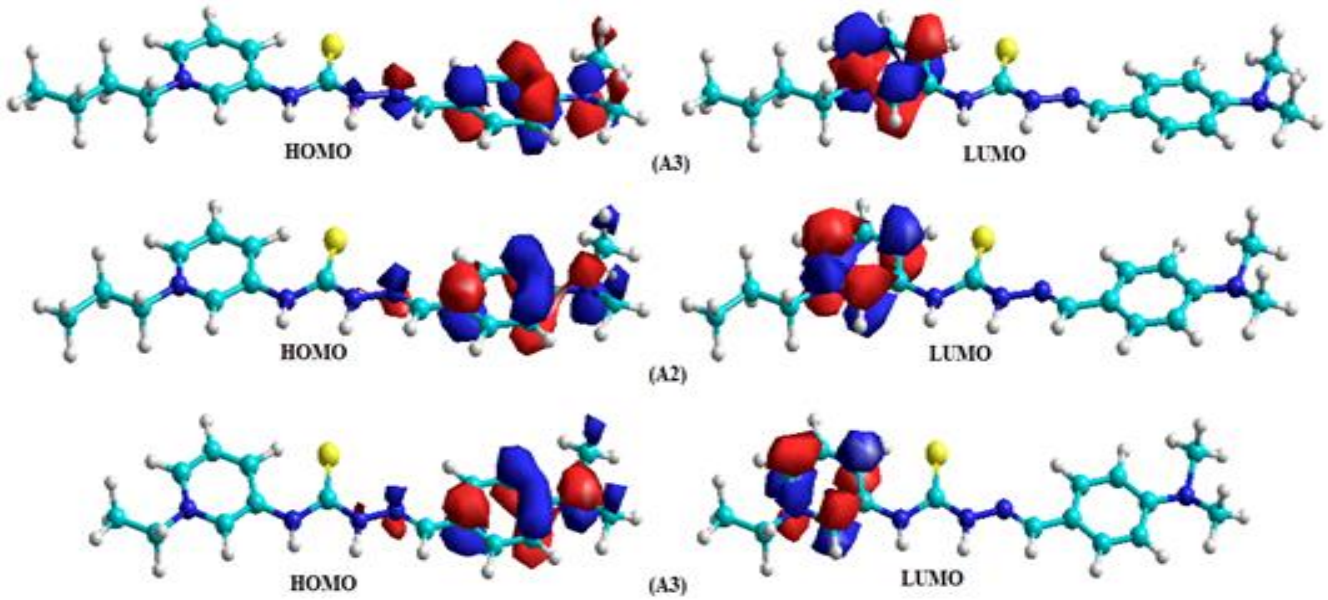

Figure 3: Using PM3 method, the proposed inhibitors of the ammonium salts (A1-A3) and their boundary distributions of molecular orbital density (HOMO and LUMO)

Therefore, the calculated HOMO energies for the pyridinium salts (A1), (A2) and (A3) are -10.1037, -10.1051,
-10.1091 eV, respectively (see Table 3). It is clearly that the HOMO energies are near in values, as well as, the values of the highest IE% and ΔG^{o}_{ads} (see Table 2). Its meaning, there is an interesting coincidence between theoretical and experimental

data. The LUMO energy is calculated to be -4.9673, -4.9748, -4.9907eV for (A1-A3), respectively (see Table 3). This means inhibitor (A3) with lowest LUMO energy can be readily to accept electrons from d-orbital of corroding surface metal by comparing with LUMO energies of (A1 and A2). The energy band gap between HOMO-LUMO energy levels is another quantum vital parameter that is needed to be put into consideration; since the smaller band gap accompanies the greater the corrosion inhibition efficiency [31]. As shown in Table 3, that (A3) has lowest band gap energy than (A1 and A2) with excellent corrosion inhibition efficiency. This suggests that the carbon chain with N atom of pyridinium ring gives flexibility for overall molecules to orient itself toward the active sites on the surface metal, that makes structural molecule of inhibitor (A3) can play a crucial role in the adsorption process on the metal surface. Furthermore, the calculated dipole moment is an important expression of non-uniform distribution of charges on various atoms in the molecule. It measures interactions of molecules in a particular chemical environment. Table 3 shows the dipole moments of the pyridinium salts (A1-A3) are in range (16-20 D) that values indicated that the feature of salt applies to these pyridinium salts. It was clear that energy of the deformability increases with the increase the value of dipole moment, making the molecule easier to be adsorbed on metal surface. Thus, as shown in Tables (2,3) that corrosion inhibition efficiency of a molecule to be high value with increasing the magnitude of dipole moment [32]. Figure 4 displays electrostatic potential maps that illustrate the varying magnitudes of computed dipole moments for the recommended inhibitors (A1-A3). Table 3 illustrates that the compounds polarizability order is A3> A2> A1, indicating that high inhibitor polarization values correspond to high inhibition efficiency. High values of polarizability facilitate the strong adsorption process of corrosion inhibitors onto the metal surface and hence, high inhibition efficiency [33]. The qualitative definition of hardness is closely related to the polarizability, since polarizability (α) is inversely proportional to the third power of the hardness values [34]. Therefore, molecule becomes more polarizable with increasing of softness (see Table 3). Since a decrease of the energy gap usually leads to easier polarization of the molecule, which decreases (LUMO– HOMO) energy gap and improves the efficiency of inhibitor [35]. Figure 4 displays electrostatic potential maps that illustrate the varying magnitudes of computed polarizability.

A molecule's tendency to transfer electrons to an electron-deficient species is indicated by the quantity of electrons moved (ΔN); the higher value of ΔN, the more probable a molecule will do that. Therefore, as organic corrosion inhibitor is examined, a greater ΔN can be indicated with a higher propensity to interact with the surface of the metal that makes sense to lead to increasing corrosion inhibition efficiency [33]. As shown in Table 3, that (A3) has highest electrons transmitted than (A1 and A2). With the findings of the experiment are in good agreement with this. One crucial indicator of an atom's or molecule's chemical reactivity is their ionization potential (I). Small ionization potential indicates strong reactivity of the atoms and molecules, while high ionization potential indicates great stability and chemical inertness [34]. The great inhibitory efficacy of (A1) is indicated by its low ionization potential (I = 10.1037 eV). With the findings of the experiment are in good agreement with this.

The chemical property that characterizes a molecule's capacity to draw electrons into itself in a covalent connection is called absolute electronegativity (χ). The molecules (A1, A2, and A3) with a large electronegativity rapidly achieve equitable distribution, as a result, high responsiveness is expected, indicating good inhibitory efficiency, according to Sanderson's electronegativity equalization principle [35]. According to Table 3, (A3) exhibits the maximum electronegativity. Thus, the highest increase in the electronegativity difference between the metal and inhibitor is seen for (A3). This is consistent with the experiment's results. Measuring molecule stability and reactivity requires knowledge of absolute hardness (η) and softness (σ) [36]. It is clear that the resistance to deformation or polarization of the electron field of atoms, ions, or molecules under mild chemical reaction perturbations is what chemical hardness essentially signifies. The energy gap between a soft molecule and a hard molecule is smaller [37]. In the current investigation, the salt (A3) has the lowest energy gap and the lowest hardness value (2.5592 eV) when compared to other created pyridinium salts.

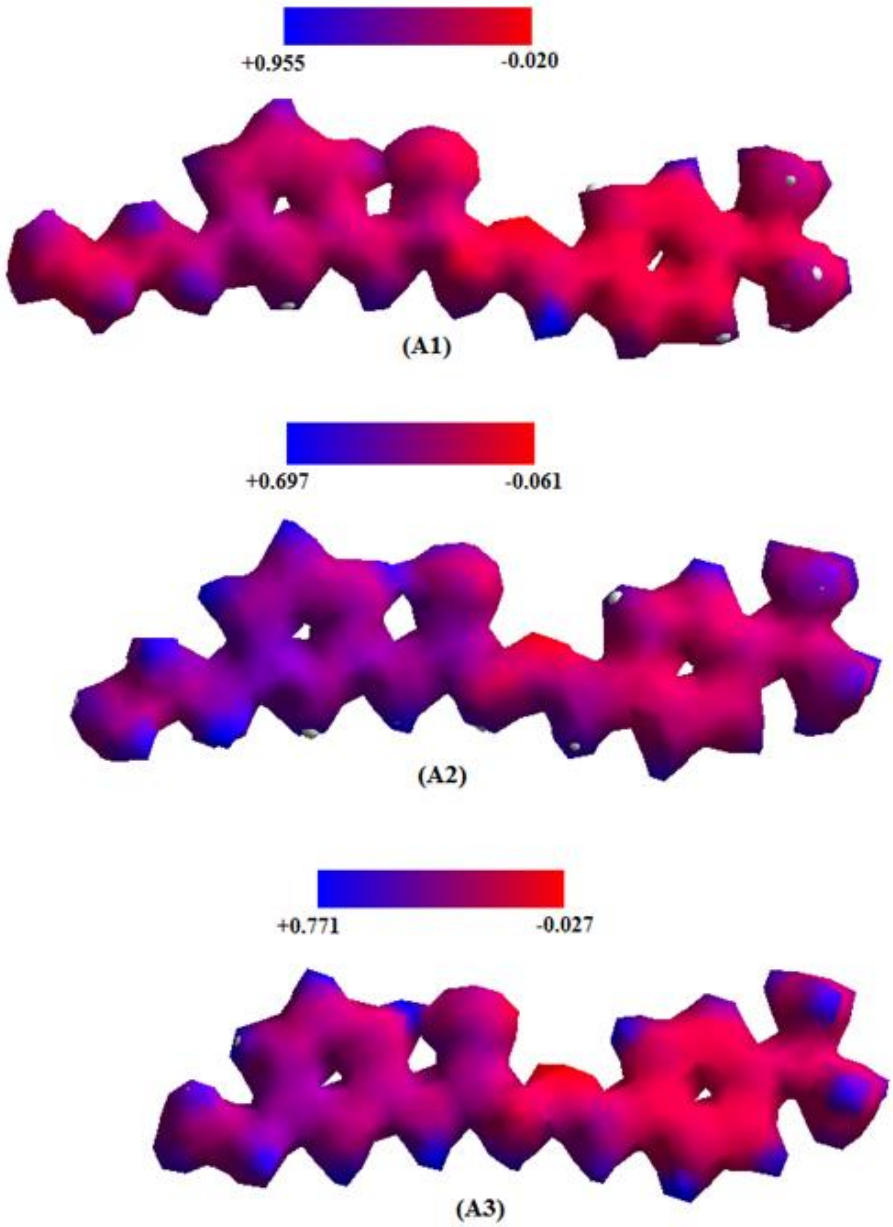

Figure 4: Electrostatic potential maps that illustrate the varying magnitudes of computed inhibitors (A1-A3) by using PM3 method.

In general, a high inhibition efficiency is predicted for the inhibitor with the lowest global hardness value (and thus the largest global softness value) [38]. Adsorption may take place at the location of the molecule where the local property softness (σ) has the maximum value in order to facilitate the easiest electron transport [39]. A softness value of 0.3907 eV^{-1}, the pyridinium salt (A3) exhibits a high level of inhibitory efficiency. This is consistent with the experiment's results. Taking account of the global electrophilicity index (ω), which quantifies a molecule's tendency to be electrophilic and the stabilization energy and the tendency of chemical species to obtain addition charge from ΔN the environment [40]. We find that the inhibitor (A3) with highest electrophilicity index value (11.1365 eV) than the other (A1 and A2), then (A3) has a high inhibition efficiency as well as, a good value free energy adsorption. This result is in good agreement with the experimental data. When assessing corrosion inhibitors, two crucial factors to take into account are the electrophilicity index (ω) and the nucleophilicity index (ε). (ω) represents the ability of inhibitor molecules to acquire electrons, whereas (ε)

represents their ability to contribute electrons. The inhibitory activity rises with increasing (ε) value and declines with decreasing (ω) value [41, 42]. In our research of molecules, the value of (ω) has reduced and the value of (ε) has increased. The strongest inhibitory action is exhibited by our compounds (A1-A3), as determined by (ε and ω) assays. Through back-donation (ΔEback-donation), the inhibitor potency and center activity are further investigated [43]. An effective inhibition process would be indicated by this type of action if $\eta > 0$ and $\Delta E_{back\text{-}donation} < 0$. This would indicate that there is a move of charge to the molecule followed by return donation to the unoccupied d-orbital of the metal atom [44]. In comparison to A1 (-0.6420 eV) and A2 (-0.6412 eV), $\Delta E_{back\ -\ donation}$ is highly advantageous for A3 (-0.6398 eV; see Table 3). The vdW volume, as well as, surface area was calculated with Hyperchem, based on Quantitative Structure Activity Relationships (QSAR), which is listed below in Table 3, demonstrating that A1 (1121 Å^3) has comparatively greater volume than A2 (1070 Å^3) and A3 (1016 Å^3). Thus, A1 offers a sizable adsorption contact area, which improves inhibitor activity. As a conclusion, the various molecule systems are showing different values of different quantum approximated chemical parameters, that maybe suggesting different interactions could be taken place between the inhibitor molecule and the metal surface.

Table 3: Quantum approximated chemical parameters of the studied pyridinium salt derivatives as corrosion inhibitors by using PM3 method.

Inhibitor	A1	A2	A3
E_{HOMO}, eV	-10.1037	-10.1051	-10.1091
E_{LUMO}, eV	*-4.9673*	-4.9748	-4.9907
ΔE, eV	5.1364	5.1303	5.1184
I, eV	10.1037	10.1051	10.1091
A, eV	4.9673	4.9748	4.9907
χ, eV	7.5355	7.5399	7.5499
η, eV	2.5682	2.5651	2.5592
σ, eV^{-1}	0.3893	0.3898	0.3907
ΔN	0.8628	0.8644	0.8676
ω, eV	11.0551	11.0814	11.1365
ε, eV^{-1}	0.0904	0.0902	0.0897
$\Delta E_{back\text{-}donation}$, eV	-0.6420	-0.6412	-0.6398
VdW, Å^3 (surface area, Å^2)	1121.85 (670.98)	1070.56 (634.39)	1016.82 (596.88)
Dipole moment (D)	16.50	18.33	20.07
Polarizability, a.u.	263.90	272.37	279.32

3.4. Molecular mechanics investigation

The three inhibitors adsorbed on the Fe (001) surface (Fe0) and their small energy adsorption patterns are displayed in Fig. 5. The electrons of the nitrogen, sulfur, and benzene rings are the adsorption sites of the inhibitors under study on the surface of Fe (001), as shown in Fig. 5. Adsorbate/substrate system interaction is strengthened when inhibitor molecules are adsorbed in a nearly flat configuration on the surface of the iron to increase covering and contact with the surface [45,46]. Studying the adsorption energies of inhibitors absorbed on iron surfaces when taking inhibition performance into account will be highly attractive, as the potency of corrosion inhibitors absorbed on iron surfaces can be described by the adsorption energy (Eads). The following equation [47] can be used to determine the adsorption energy in a solution.

$$E_{ads.} = E_{total\ /\ complex\ (Fe-Inh.)} - \left(E_{total/Fe} + E_{total\ /Inh.}\right) \quad \ldots(8)$$

The average adsorption energy of the acquired equilibrium configurations was used to compute the energies of adsorption in the present study. The E_{ads} acquired are (-89.33, 87.32 and -81.87 kJ/mol) for A1, A2, and A3, respectively (see Table 4) [48]. Since the adsorption energies are shown to be negative, spontaneous adsorption is predicted [49]. Essentially, the greater the contact between the blocker and the metal surface, the greater the absolute value of E_{ads} [50]. A1 clearly shows superior inhibitory qualities for mild steel than A2 and A3, with larger absolute values of Eads than the latter

two. These findings are consistent with experimental evidence [51]. The relative energy of the complex creation by the subtracted portion of the total heat of synthesis for each individual component is shown in Figure 6 (see Table 4). Correlation between the theoretical E_{ads} values and the results of measurements of electrochemical values, the values of ΔG^{o}_{ads}, that follow the order A2≅A1>A3. This is due to the following factors: A1 and A2 have a larger molecular size than A3 with (it could be) a large effect of carbon chain on orientation the molecular system on metal surface, that allowing A1 and A2 to cover a larger area over the metal surface that causes high values of IE%, ΔG^{o}_{ads} and E_{ads}.

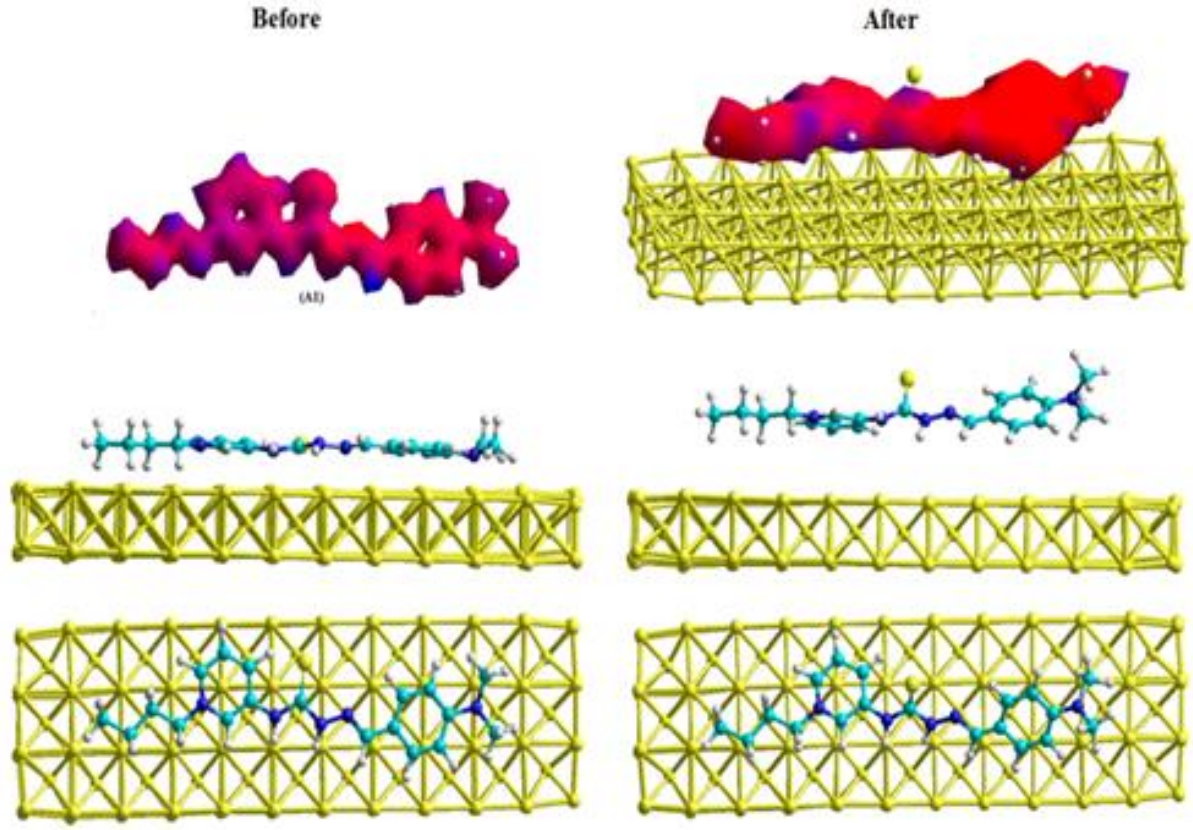

Figure 5: Side and top views of most stable adsorption configurations and electrostatic potential maps for A1 inhibitor on Fe (001) surface (Fe^0) (before and after simulation).

Table 4: Quantum chemical properties of the proposed inhibitors with metal surface using Mm+ method were computed

Component	Total energy, (kJ/mol)	E_{ads}, (kJ/mol)
A1	147.40	-89.33
A2	144.90	-87.32
A3	141.64	-81.87
Fe crystal	21402.05	
Complex(Fe-InhA1)	21460.12	
Complex(Fe-InhA2)	21459.63	
Complex(Fe-InhA3)	21461.82	

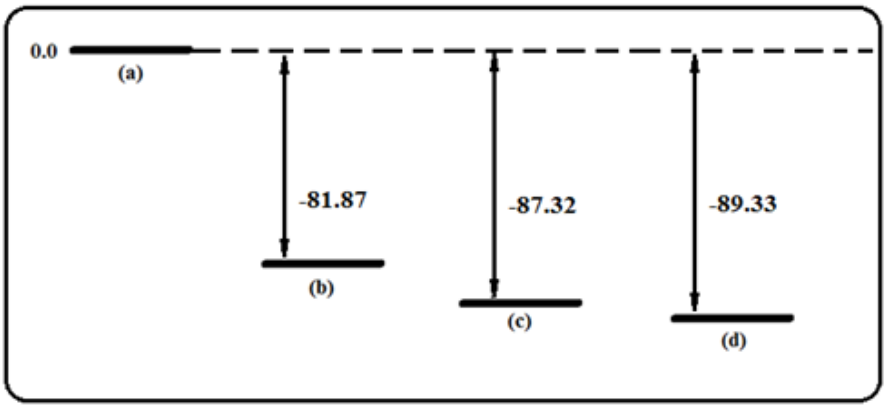

Figure 6: Diagram of proportional adsorption energy for the production of complexes. (a) (Inh +Fe crystal), (b) for complex (Fe-InhB5), (c) for complex (Fe-InhB6) and (d) for complex (Fe-InhB4); energies are in kJ mol^{-1}.

We suggested another molecular simulation with a charged iron upper surface (Fe^{II}) to calculate the three inhibitors' configurations for minimal energy adsorption (A1, A2 and A3) adsorbed on the Fe (001) surface (Fe^{II}) are shown in Fig. 7. The E_{ads} obtained are (-86.93, -83.79 and -81.35 kJ/mol) for A1, A2 and A3, respectively (see Table 5).

Table 5: Calculated quantum chemical parameters of the suggested inhibitors with charged metal surface, using Mm+ method.

Component	Total energy, (kJ/mol)	E_{ads}, (kJ/mol)
A1	147.40	-86.93
A2	144.90	-83.79
A3	141.64	-81.35
Fe^{II} crystal	21133.46	
Complex(Fe^{II}-InhA1)	21193.93	
Complex(Fe^{II}-InhA2)	21194.57	
Complex(Fe^{II}-InhA3)	21193.75	

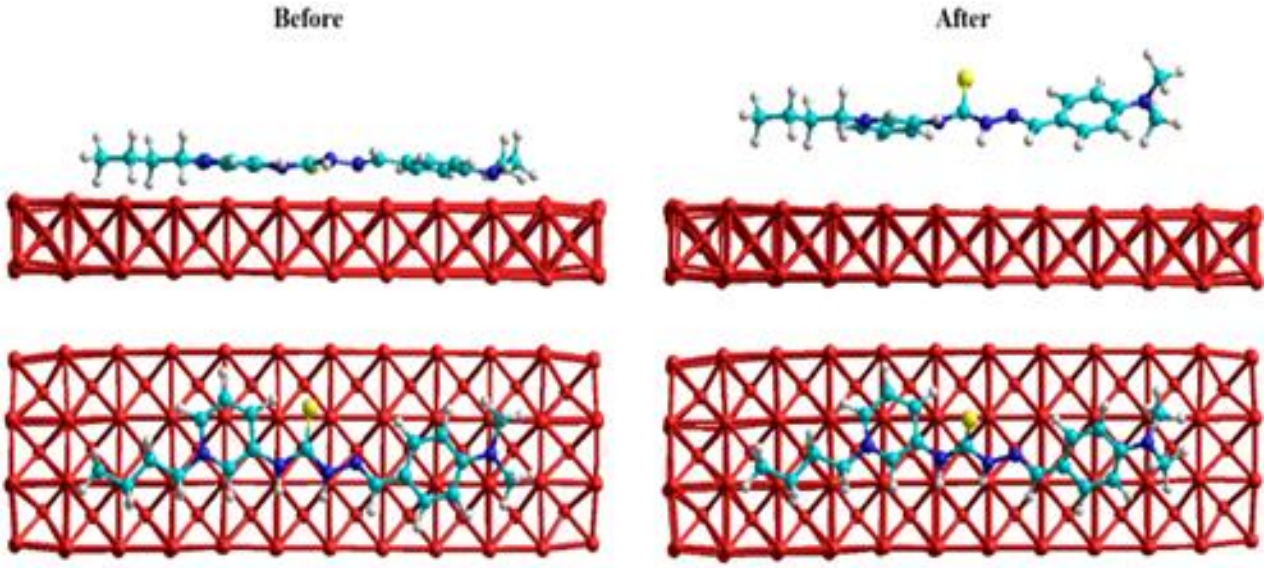

Figure 7: Side and top views of most stable adsorption configurations and electrostatic potential maps for inhibitor A1on Fe (001) surface (Fe^{II}) (before and after simulation).

It's clear from E_{ads} data of Tables (3, 4) that the adsorption process by inhibitor molecule on the charged iron upper surface was approximately the same as uncharged iron upper surface with inhibitor molecule. That explains that adsorption process between molecular system and the metal surface are strong in case of charged iron upper surface or uncharged iron upper surface. In addition, the relationship between experimental data of ΔG^{o}_{ads} and theoretical E_{ads} calculations are found to make conclusion that two cases of protection for metal surface can occur synergistically by inhibitor molecules with charged and uncharged iron surface, (see Figure 8).

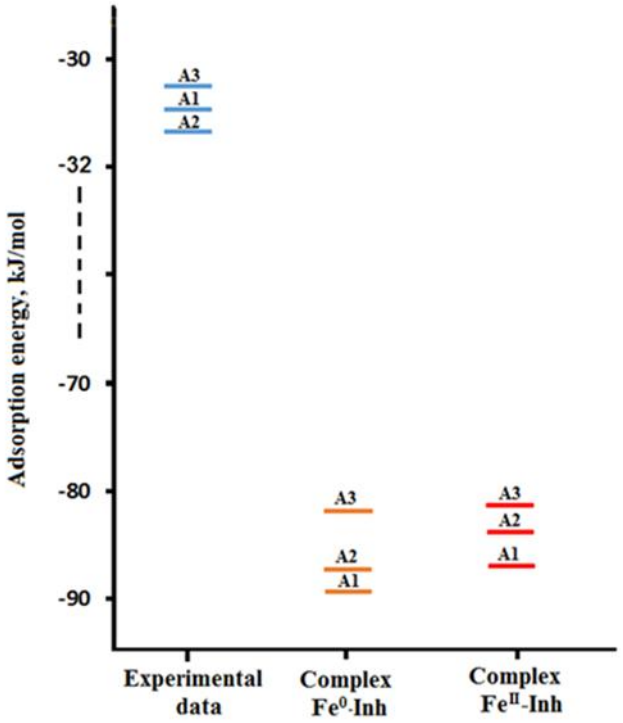

Figure 8: Adsorption energy diagram for the complexes formation between inhibitor molecule and uncharged and charged iron surface.

3.5. The mechanism of corrosion inhibition

Finally, the mechanism of corrosion inhibition for the present work is physicochemical characteristics over Fe surface. In the light of the experimental research and theoretical computations, it is suggested that changing the electronic environment of the metal surface might be used to demonstrate adsorption. The inhibitory effect of the pyridinium salts on the iron surface is shown in Fig. 9. Numerous investigations have demonstrated that the surface of metal in an acidic solution lacks electrons [52]. The inhibitor's ability to be adsorbed on the surface of metal is explained by the ability of specific function groups to connect to the inhibitor molecules on the surface of metal. The creation of a protective coating of molecules of inhibitors on the metal/solution contact boosts the effectiveness of inhibition when the concentration of the inhibitor is increased. The change of the electronic environment for Fe surfaces encourages organic inhibitor molecule to be adsorption, resulting a thin layer of organic inhibitor molecules in the solution. Because the N and S electrons are not shared, these organic salt compounds can combine in solution. Molecules of organic material may have a physiosorbed effect on the surface of metal as a result of electrostatic interaction [53]. The organic molecule could be absorbed by an imagined process on the metal/acid mixture interaction. In Fig. 9, the following processes are shown: (i) physisorption, or the electrostatic attraction of protonated organic molecules that inhibit with currently adsorbed ions; (ii) chemisorption or physisorption, is the interaction of charged particles and unpaired electrons of the heteroatoms with the unoccupied d-orbital of iron surface atoms; and the relationship between the d-electron of the iron surface atom and the unoccupied orbital of the molecule that inhibits (retro-donation).

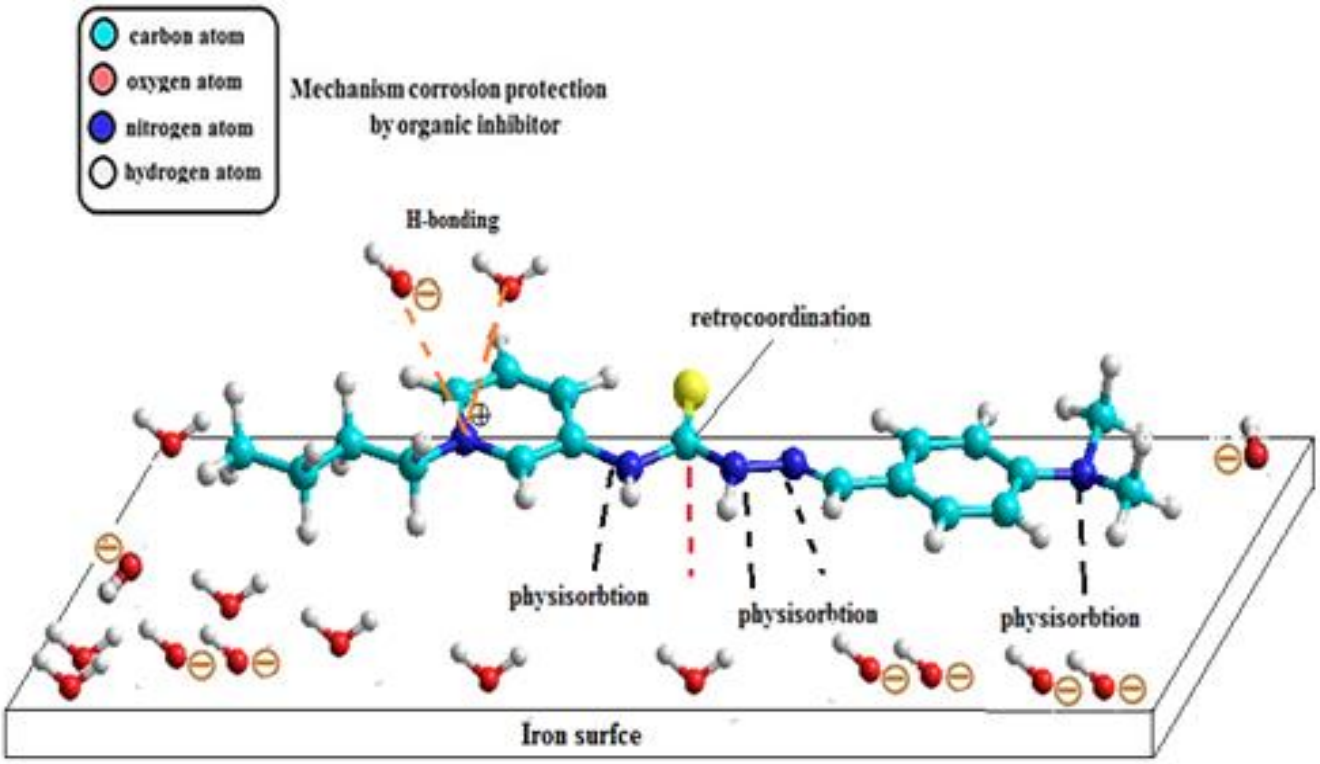

Figure 9: Mechanism of relationship between inhibitor molecules and the mild steel surface environment that has been proposed.

4. Conclusions

The use of pyridinium salts (A1-A3) as organic corrosion inhibitors on the iron metal surface in a solution of 1 M H_2SO_4 at room temperature was successful. The synthesized inhibitor compounds exhibited significant inhibitory effects, as indicated by the efficiency inhibition (IE%) data. The physical process of adsorption was influencing the free energy adsorption readings (A1, A2, and A3), which provided crucial information to clarify the natural of the organic molecules' interactions with the metal. The correlation between theoretical data via quantum molecular orbital calculations and the outcomes of the three inhibitors under study were taken into consideration. Theoretical simulations helped clarify the mechanism of the relationship between the organic inhibitor of corrosion and the iron surface.

Acknowledgments: The authors thank Al-Nahrain University for supporting.

Funding: This work is Self-funded.

Conflicts of Interest: The authors state that they have no conflicts of interest to declare.

References

[1] Desai, P.D.; Pawar, C.B.; Avhad, M.S.; More, A.P.; "Corrosion inhibitors for carbon steel: A review". Vietnam J. Chem., 61(1): 15-42, 2023.

[2] Ali, T.R.; Salman, T.A.; Shihab, M.S.; "Pomelo leaves extract as a green corrosion inhibitor for carbon steel in 0.5 M HCl". Int J. corros. Scale Inhib., 10(4): 1729-1747, 2021.

[3] Honarvar Nazari, M.; Shihab, M.S.; Havens, E.A.; Shi, X.; "Mechanism of corrosion protection in chloride solution by an apple-based green inhibitor: experimental and theoretical studies". J Infrastruct Preserv Resil, 1: 1-19, 2020.

[4] Khudhair, Z.T.; Shihab, M.S.;. "Study of Synergistic Effect of Some Pyrazole Derivatives as Corrosion Inhibitors for Mild Steel in 1 M H_2SO_4". Surf. Eng. Appl. Electrochem, 56: 601-609, 2020.

[5] Shihab, M.S.; Mahmood, A.F.; "Experimental and theoretical study of some N-pyridinium salt derivatives as corrosion inhibitors for mild-steel in acidic media". Russ. J. Appl. Chem, 89: 505-516, 2016.

[6] Ma, I.W.; Ammar, S.; Kumar, S.S.; Ramesh, K.; Ramesh, S.; "A concise review on corrosion inhibitors: types, mechanisms and

electrochemical evaluation studies". J Coat Technol Res, 19: 241–268, 2022.

[7] Mainier, F.B.; Guimar, P.I.C.; "Use of corrosion inhibitor in solid form to prevent internal corrosion of pipelines and acidification process". J. mater. sci. chem. eng, 2: 1-6, 2014.

[8] Sun, S.; Li, Y.; Gao, K.; Cheng, L.; Yang, X.; Liao, R.; "Synthesis of a Hydroxyl-Containing Corrosion Inhibitor and Its Inhibitory Performance on N80 Steel in Hydrochloric Acid Solution". Coatings, 12(12): 1975, 2022.

[9] Kareem, R.; Shihab, M.S.; "Study new pyridine derivatives as corrosion inhibitors for mild steel in an acidic media". Nahrain J. Sci., 24(3): 1-8, 2021.

[10] Qi, W.; Huang, Y.; Ma, Y.; Yu, Z.; Zhu, X.; "Developing novel imidazoline-modified glucose derivatives as eco-friendly corrosion inhibitors for Q235 steel". RSC Adv., 13(20): 13516-13525, 2023.

[11] Vaszilcsin, C.G.; Putz, M.V.; Kellenberger, A.; Dan, M.L.; "On the evaluation of metal-corrosion inhibitor interactions by adsorption isotherms". J. Mol. Struct, 1286: 135643, 2023.

[12] Okafor, C.S.; Anadebe, V.C.; "Onukwuli, O.D., 2019. Experimental, statistical modelling and molecular dynamics simulation concept of sapium ellipticum leaf extract as corrosion inhibitor for carbon steel in acid environment". S. Afr. J. Chem, 72: 164-175, 2019.

[13] Ahmed, M.M.; Shihab, M.S.; "Pyridinium Bromide Derivatives as Corrosion Inhibitors For Mild Steel in 1M H_2SO_4". Egypt. J. Chem, 66(2): 63-72, 2023.

[14] Cai, C.; Yu, C.; Taryba, M. G.; Alves, M. M.; Song, R.; Cui, Y.; Montemor, M. F.; "Revealing the early electrochemical corrosion behavior of Mg-Zn-Zr-Nd alloys in a simulated orthopedic environment". J. Mater. Res. Technol., 35: 4217–4230, 2025.

[15] Aslam, J.; Aslam, R.; Alrefaee, S. H.; Mobin, M.; Aslam, A.; Parveen, M.; Hussain, C. M.; "Gravimetric, electrochemical, and morphological studies of an isoxazole derivative as corrosion inhibitor for mild steel in 1M HCl". Arab. J. Chem, 13(11): 7744-7758, 2020.

[16] Kumari, P.; Lavanya, M.; "Optimization of inhibition efficiency of a schiff base on mild steel in acid medium: electrochemical and RSM approach". J. Bio. Tribo Corros, 7(3): 110, 2021.

[17] Fouda, A.E.A.S.; El-Askalany, A.H.; Molouk, A.F.; Elsheikh, N.S.; Abousalem, A.S; "Experimental and computational chemical studies on the corrosion inhibitive properties of carbonitrile compounds for carbon steel in aqueous solutions". Sci Rep, 11(1): 21672, 2021.

[18] Espinoza-Vázquez, A.; Rodríguez-Gómez, F.J.; Martínez-Cruz, I.K.; Ángeles-Beltrán, D.; "Adsorption and corrosion inhibition behaviour of new theophylline–triazole-based derivatives for steel in acidic medium". R. Soc. Open Sci, 6(3): 181738, 2019.

[19] Stewart, J.J.; "Optimization of parameters for semiempirical methods II. Applications". J. Comput. Chem., 10(2): 221-264, 1989.

[20] Pahari, B.; Chakraborty, S.; Sengupta, B.; Chaudhuri, S.; Martin, W.; Taylor, J.; Henley, J.; et.al.; "Biophysical characterization of genistein in its natural carrier human hemoglobin using spectroscopic and computational approaches". Food Sci. Nutr. 4(8): 83-92, 2013.

[21] Hadisaputra, S.; Purwoko, A. A.; Savalas, L. R. T.; Prasetyo, N.; Yuanita, E.; Hamdiani, S.;"Quantum chemical and Monte Carlo simulation studies on inhibition performance of caffeine and its derivatives against corrosion of copper". Coatings, 10(11): 1086, 2020.

[22] Khadom, A.A.; Mahmmod, A.A.; "Quantum chemical and mathematical statistical calculations of phenyltetrazole derivatives as corrosion inhibitors for mild steel in acidic solution: a theoretical approach". Results Eng., 16: 100741, 2022.

[23] Al-Amiery, A. A.; Mohamad, A. B.; Kadhum, A. A. H.; Shaker, L. M.; Isahak, W. N. R. W.; Takriff, M. S.; "Experimental and theoretical study on the corrosion inhibition of mild steel by nonanedioic acid derivative in hydrochloric acid solution". Sci Rep, 12(1): 4705, 2022.

[24] Hocquet, A.; Langgård, M.; "An evaluation of the MM+ force field". J. Mol. Model, 4: 94-112, 1998.

[25] Pepperhoff, W.; Acet, M.; Pepperhoff, W.; "Substitutional alloys of iron. In Constitution and Magnetism of Iron and its Alloys". Eng. Mater, 83-145, 2001.

[26] Chauhan, D.S.; Verma, C.; Quraishi, M.A.; "Molecular structural aspects of organic corrosion inhibitors: Experimental and computational insights". J. Mol. Struct., 1227: 129374, 2021.

[27] Ogunleye, O. O.; Arinkoola, A. O.; Eletta, O. A.; Agbede, O. O.; Osho, Y. A.; Morakinyo, A. F.; Hamed, J. O.; "Green corrosion inhibition and adsorption characteristics of Luffa cylindrica leaf extract on mild steel in hydrochloric acid environment". Heliyon, 6(1): 1-12, 2020.

[28] Rodríguez, J.A.; Cruz-Borbolla, J.; Arizpe-Carreón, P.A.; Gutiérrez, E.; "Mathematical models generated for the prediction of corrosion inhibition using different theoretical chemistry simulations". Materials, 13(24): 5656, 2020.
[29] Chen, L.; Lu, D.; Zhang, Y.; "Organic compounds as corrosion inhibitors for carbon steel in HCl solution: a comprehensive review". Materials, 15(6): 2023, 2022.
[30] Al-Baghdadi, S.B.; Hashim, F.G.; Salam, A.Q.; Abed, T.K.; Gaaz, T.S.; Al-Amiery, A.A.; Kadhum, A.A.H.; et.al.; "Synthesis and corrosion inhibition application of NATN on mild steel surface in acidic media complemented with DFT studies". Results Phys., 8: 1178-1184, 2018.
[31] Verma, C.; Obot, I. B.; Bahadur, I.; Sherif, E. S. M.; Ebenso, E. E.; "Choline based ionic liquids as sustainable corrosion inhibitors on mild steel surface in acidic medium: Gravimetric, electrochemical, surface morphology, DFT and Monte Carlo simulation studies". Appl. Surf. Sci, 457: 134-149, 2018.
[32] Yadav, D.K.; and Quraishi, M.A.; "Electrochemical investigation of substituted pyranopyrazoles adsorption on mild steel in acid solution". Ind. Eng. Chem. Res, 51(24): 8194-8210, 2012.
[33] Elmi, S.; Foroughi, M.M.; Dehdab, M.; Shahidi-Zandi, M.; "Computational evaluation of corrosion inhibition of four quinoline derivatives on carbon steel in aqueous phase". Iran. J. Chem. Chem. Eng., 38(1): 185-200, 2019.
[34] Ghanty, T.K.; Ghosh, S.K.; "Correlation between hardness, polarizability, and size of atoms, molecules, and clusters". J. Phys. Chem., 97(19),: 4951-4953, 1993.
[35] Shahen, S.; Kabel, K. I.; Kamel, L. A.; Abou-Shahba, R. M.; El-Shenawy, A.; "Preparation and Assessment of Water Soluble Hyperbranched Polymers Based on Polyamide as Corrosion Inhibitor for Petroleum Application". J. Sci. Res., 34(1): 360-372, 2017.
[36] Espinoza-Vázquez, A.; Rodríguez-Gómez, F.J.; Martínez-Cruz, I.K.; Ángeles-Beltrán, D.; Negrón-Silva, G.E.; Palomar-Pardavé, M.; Romero, L.L.; et al.; "Adsorption and corrosion inhibition behaviour of new theophylline–triazole-based derivatives for steel in acidic medium". R. Soc. Open Sci., 6(3): 181738, 2019.
[37] Abbas, M.A.; Ismail, A.S.; Zakaria, K.; El-Shamy, A.M.; El Abedin, S. Z.; "Adsorption, thermodynamic, and quantum chemical investigations of an ionic liquid that inhibits corrosion of carbon steel in chloride solutions". Sci. Rep., 12(1): 12536, 2022.
[38] Gad, E.A.; Azzam, E.M.S.; Halim, S.A.; "Theoretical approach for the performance of 4-mercapto-1-alkylpyridin-1-ium bromide as corrosion inhibitors using DFT". Egypt. J. Pet, 27(4): 695-699, 2018.
[39] Çakır, B.; Emregül, K.C.; "A theoretical approach to the inhibitive effect of two new Schiff base compounds". Commun. Fac. Sci. Univ. Ank. Ser. B, 64(1): 1-19, 2022.
[40] Miar, M.; Shiroudi, A.; Pourshamsian, K.; Oliaey, A. R.; Hatamjafari, F.; "Theoretical investigations on the HOMO–LUMO gap and global reactivity descriptor studies, natural bond orbital, and nucleus-independent chemical shifts analyses of 3-phenylbenzo [d] thiazole-2 (3 H)-imine and its para-substituted derivatives: Solvent and substituent effects". J. Chem. Res., 45(1-2): 147-158, 2021.
[41] Kathirvel, K.; Thirumalairaj, B.; Jaganathan, M.; "Quantum chemical studies on the corrosion inhibition of mild steel by piperidin-4-one derivatives in 1 M H_3PO_4". Open J. Met., 4: 73-85, 2014.
[42] Hachani, S.E.; Necira, Z.; Mazouzi, D.E.; Nebbache, N.; "Understanding the inhibition of mild steel corrosion by dianiline schiff bases: A DFT investigation". Acta Chim. Slov., 65(1): 183-190, 2018.
[43] Oguike, R. S.; Oni, O.; Barambu, A. U.; Balarak, D.; Buba, T.; Okeke, C. U.; Momoh, L.S.; et.al.; "Computational stimulation and experimental study on corrosion inhibition qualities of Emilia sonchifolia leaf extract for copper (CU131729) in hydrochloric acid". J. Comput. Chem., 9(1): 18-36, 2020.
[44] Guo, L.; Ren, X.; Zhou, Y.; Xu, S.; Gong, Y.; Zhang, S.; "Theoretical evaluation of the corrosion inhibition performance of 1, 3-thiazole and its amino derivatives". Arab. J. Chem., 10(1): 121-130, 2017.
[45] Javadian, S.; Darbasizadeh, B.; Yousefi, A.; Ektefa, F.; Dalir, N.; Kakemam, J.; "Dye-surfactant aggregates as corrosion inhibitor for mild steel in NaCl medium: Experimental and theoretical studies". J. Taiwan Inst. Chem. Eng., 71: 344-354, 2017.
[46] Mahdavian, M.; Tehrani-Bagha, A.R.; Alibakhshi, E.; Ashhari, S.; Palimi, M. J.; Farashi, S.; Ektefa, F. "Corrosion of mild steel in hydrochloric acid solution in the presence of two cationic gemini surfactants with and

without hydroxyl substituted spacers". Corros. Sci., 137: 62-75, 2018.

[47] Zhang, Z.; Tian, N.; Li, X.; Zhang, L.; Wu, L.; Huang, Y.; "Synergistic inhibition behavior between indigo carmine and cetyl trimethyl ammonium bromide on carbon steel corroded in a 0.5 M HCl solution". Appl. Surf. Sci., 357: 845-855, 2015.

[48] Zhang, F.; Liu, S.; Zhang, X.; Xu, C.; Liu, S.; Wang, J.; "Research on 1, 10-phenanthroline quaternary ammonium salt composite corrosion inhibitors for oilfield acidizing at high temperatures and high HCl concentrations". Geoenergy Sci. Eng, 225: 211663, 2023.

[49] Galai, M.; Rbaa, M.; Ouakki, M.; Abousalem, A.S.; Ech-Chihbi, E.; Dahmani, K.; Dkhireche, N.; "Chemically functionalized of 8-hydroxyquinoline derivatives as efficient corrosion inhibition for steel in 1.0 M HCl solution: Experimental and theoretical studies". Surf. Interfaces, 21: 100695, 2020.

[50] Murmu, M.; Saha, S.K.; Murmu, N.C.; Banerjee, P.; "Effect of stereochemical conformation into the corrosion inhibitive behaviour of double azomethine based Schiff bases on mild steel surface in 1 mol L− 1 HCl medium: An experimental, density functional theory and molecular dynamics simulation study". Corros. Sci., 146: 134-151, 2019.

[51] Bahlakeh, G.; Ramezanzadeh, B.; Dehghani, A.; Ramezanzadeh, M.; "Novel cost-effective and high-performance green inhibitor based on aqueous Peganum harmala seed extract for mild steel corrosion in HCl solution: detailed experimental and electronic/atomic level computational explorations". J. Mol. Liq., 283: 174-195,2019.

[52] Olasunkanmi, L.O.; Ebenso, E.E.; "Experimental and computational studies on propanone derivatives of quinoxalin-6-yl-4, 5-dihydropyrazole as inhibitors of mild steel corrosion in hydrochloric acid". J Colloid Interface Sci., 561: 104-116, 2020.

[53] Obot, I.B.; Obi-Egbedi, N.O.; "Adsorption properties and inhibition of mild steel corrosion in sulphuric acid solution by ketoconazole: experimental and theoretical investigation". Corros. Sci., 52(1): 198-204, 2010.